International Journal of Scientific Engineering and Science
Volume 2, Issue 4, pp. 63-73, 2018. ISSN (Online): 2456-7361

Generation of Regular and Chaotic Pulses via an Electrical Oscillator Forced by an External Periodic Signal

Guy Bertrand NDOMBOU[1], Fabien KENMOGNE[2], Samuel NOUBISSIE[2], David YEMELE[3], Jean Blaise TEGUIA[4], Anaclet FOMETHE[3]

[1]Laboratory of Electronics and Signal Processing, Faculty of Science, University of Dschang, Po Box 067, Dschang, Cameroon
[2]Laboratory of Modeling and Simulation in Engineering, Biomimetics and Prototype, Faculty of Science, University of Yaoundé I, Po Box 812, Yaoundé Cameroon
[3]Laboratoire de Mécanique et de Modélisation des Systèmes Physiques L2MSP, Faculté des Sciences, Université de Dschang, B.P. 067, Dschang, Cameroon
[4]Laboratoire d'automatique et Informatique, IUT Bandjoun, Université de Dschang, Cameroon

Abstract—*The dynamics of the newly chaotic pulse oscillator, driven by an external periodic signal voltage is strongly investigated. This particular forced oscillator has broad range applications in electronic and telecommunication, such as the generation of trains of regular and chaotic pulses. Although regular pulses are useful for the modulation of signals, the chaotic one can be used for the signal masking and modulations. Based on the appropriate selection of the state variables, a mathematical model is derived for the analytical description of the system's dynamics. This mathematical model is used to seek the equilibrium points and study their stabilities. Applying next the two parameters perturbation methods, the periodic solution is found and proved to be sensitive to nonlinearity parameter and the external signal voltage's amplitude. Through numerical investigations, the route to chaos by the periodic doubling is observed, as well as other complex behavior such as the generation of pulse like signals. In order to verify theoretical and numerical studies, Pspice simulations and real experiments are performed and compared, showing a very good agreement between theory and experiments.*

Keywords— *Non-autonomous oscillator; period-doubling, train of regular pulse; train of chaotic pulse.*

I. INTRODUCTION

Since the famous discovery of soliton by John Scott Russell and the modeling of its mathematical expressions, as well as equation admitting it as solution, namely the Korteweg-de Vries (KdV), the sine Gordon and the nonlinear Schrödinger equations, many researches have been devoted to its potential applications in several physical branches and more precisely in optical [1,2] and electronic [3,4] communications. In communication systems, one usually uses high frequency pulses signal as a carrier to modulate the information to be transmitted in the form of modulated impulses [5], leading to the fact that the transmitted information usually isn't secured to pirate access. To solve this problem, the chaotic systems have been introduced and proved to be adequate tools in secured communication.

Recently, the transmission of information via chaotic carriers had been proved to be a significant application in telecommunication technology and have received particular attention [6]. Due to the intention to have information which can be the most secure, several kinds of chaos have been experimented, going to simply chaos to hyper-chaos among others [7-9]. It has been proved that each kind of chaos can only be generated by a specific type of oscillator, being it autonomous or driven. Although certain cases of autonomous oscillators, such as the Colpits, Lorentz and Chua oscillators, have been proved to have riches dynamical behaviors, the driven cases of these oscillators are richer than the autonomous one [10] and this, because of the fact that the time dependency of the driven signal voltage introduces one more degree of freedom in the system.

Particularly, some oscillators like the Duffing one can't generate signals without being driven. The particularity of the Duffing type chaotic oscillator is that oscillations vanish when the driven signal voltage is removed or not chosen condemnably, which is a serious problem. This is why in order solve this problem, A. Tamasevicius and coworkers [11] have built its autonomous version, named autonomous Duffing-Holmes (ADH) Type Chaotic Oscillator, which is able to generate chaotic or regular oscillations without being driven. According the equation obtained by analyzing this ADH chaotic oscillator as we shall see in present paper, the obtained Duffing-Holmes equation, which is the autonomous version of the Duffing equation contains terms of third order time derivative, which is known as the Jerk equation [12]. The query here is what would be the behavior of the driven case of this new version of ADH chaotic oscillator? One may wonder if this system driven by an external periodic signal voltage can generate chaotic pulses or impulses, useful in communication to propagate secured signals, which does not need to combine both chaotic circuits and pulse generator.

This is why in the present paper we have considered the driven version of this ADH chaotic oscillator, and emphasize some of its behaviors, which can't be obtained with the autonomous one. Thus the paper is organized as follow: In Section 2 we present the circuit under consideration, and derive its equations of state. Next in Section 3, we seek the equilibrium points and we study theirs stabilities criteria,

International Journal of Scientific Engineering and Science
Volume 2, Issue 4, pp. 63-73, 2018. ISSN (Online): 2456-7361

following by the analytical investigation of the periodic solution of the system equation through the two parameters perturbations method [13]. Next in Section 4, we use numerical methods to find the parameters ranges leading to the chaotic behavior of the system. Finally, Pspice simulations and real experiments are performed in Section 5 in order to confirm the validity of analytical and numerical investigations.

II. Circuit Description and State Equation

2.1. Circuit Description

We consider here the autonomous nonlinear oscillator proposed more recently by A Tamasevicius and coworkers [12] experimenting the autonomous version of the Duffing-Holmes type chaotic oscillator, but which is driven by an external sinusoidal signal voltage as depicted in Fig. 1. This oscillator contains three different stages, each containing the operational amplifiers OA_1, OA_2 and OA_3. The first stage containing OA_1, the pair of diodes (D_1 and D_2), the resistors R, R_1, R_2 and R_3, the inductor with inductance L. This pair of diodes is responsible of the nonlinear character of the oscillator under consideration and is governed by the following current voltage characteristic equation:

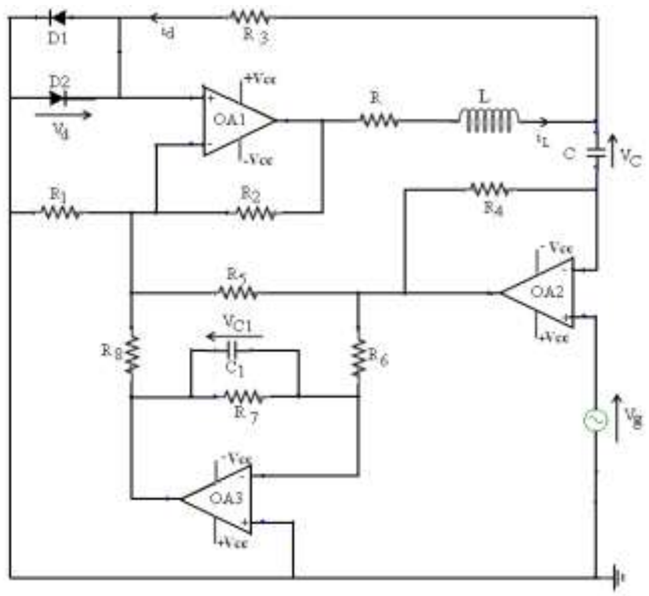

Fig. 1. Circuit diagram of the Duffing-Holmes chaotic pulse oscillator, driven by the low frequency signal generator V_g.

$$i_d = 2I_s \sinh\left(\frac{v_d}{\eta V_T}\right) \tag{1}$$

Which is derived from the Shottky diode equation [6]. Where I_s *is* the saturation current of the junction, V_d the voltage difference across this pair of diode and V_T *is* the thermal voltage. This thermal voltage is proportional to absolute temperature and takes the value $26mV$ at room temperature, that is at $293K$, while η, with $1 < \eta < 2$ is the ideality factor of the diode. The operational amplifier OA_2 contains in its negative loop the resistor R_4 and the capacitor C, which assume the connection between the two first's stages, and in the positive, the supplied sinusoidal signal voltage generator with the voltage V_g related to time t as:

$$V_g = V_0 \cos(\omega t) \tag{2}$$

V_0 being the amplitude and ω the driven signal angular frequency. This external signal voltage, we shall see introduces new phenomenon in the system as compared to previous works. OA_3 contains in negative loop the resistors R_i, with $i = 5,\ldots,8$, and the capacitor C_1. In order to simplify our studies, all operational amplifiers are supposed to be ideal (meaning that they operate in their linear regions), that is $V_+ = V_- = 0$.

Unlike many other chaotic circuits, the components values are not critical, and the circuit described here was constructed in real experiments as shown in Fig. 2, with the following arbitrary values of electronic components:

$$R_1 = 30k\Omega,\ R_2 = 100\Omega - 10k\Omega\,(\text{tuneable}),\ R_3 = 30k\Omega,\ R_4 = 820\Omega,\ R_5 = 75k\Omega$$
$$R_5 = 75k\Omega,\ R_6 = R_7 = 10k\Omega, R_8 = 20k\Omega,\ R = 20\Omega,\ C_1 = 20nF, L = 19mH,$$
$$C = 470nF. \tag{3}$$

The nonlinear diode used is the D1N4148 model with the characteristics is: $\eta = 1.9$, $VT = 6mV$ and $Is = 2.682\ nA$.

2.2 Equation of state and dynamics.

The Kirchhoff's laws applied to the oscillator shown in Fig. 1 lead to the following set of nonlinear ordinary differential equations governing the dynamics of the system:

$$\begin{cases} C\dfrac{dV_d}{dt} = \left[(i_L - i_d) + C\dfrac{dV_g}{dt}\right] \Big/ \left(1 + R_3\dfrac{di_d}{V_d}\right), \\ C_1\dfrac{dV_{C1}}{dt} = \dfrac{R_4}{R_6}(i_L - i_d) - \dfrac{V_{C1}}{R_7} - \dfrac{V_g}{R_6}, \\ L\dfrac{di_L}{dt} = \left(\dfrac{R_2R_4}{R_5} - R\right)i_L - \left(\dfrac{R_2R_4}{R_5} + R_3\right)i_d - \dfrac{R_2V_{C1}}{R_8} + \\ \qquad \left(\dfrac{R_2}{R_1} + \dfrac{R_2}{R_5} + \dfrac{R_2}{R_8}\right)V_d - \dfrac{R_2V_g}{R_5}, \end{cases} \tag{4}$$

where V_{C_1} is the voltage difference across the capacitor C_1, while i_L is the current flowing through the linear inductor. The voltage difference V_d across the pair of nonlinear diode is related to the voltage difference V_c across the capacitor C as:

$$V_c = V_d + R_3 id - V_g \tag{5}$$

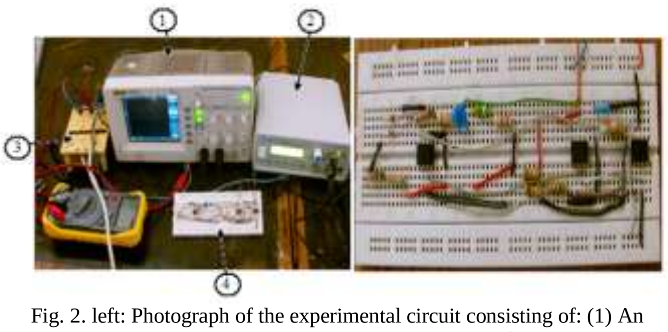

Fig. 2. left: Photograph of the experimental circuit consisting of: (1) An oscilloscope necessary to visualize signals, (2) The low frequency signal generator used to force the oscillator, (3) A source of operational amplifiers polarizations, and (4) the corresponding oscillator's circuit depicted in Fig.1, which is zoomed in the right.

It is convenient, accounting to (1) to rewrite equation (4) in the simplest dimensionless form as:

$$
\begin{cases}
\dot{x} = \left(z - p\sinh(x) - pA_0\Omega\sin(\Omega\tau)\right) / \left(1 + \dfrac{p}{\gamma_3}\cosh(x)\right) \\
\dot{y} = \varepsilon\left[\dfrac{\gamma_6}{\gamma_4}\left(z - p\sinh(x)\right) - \gamma_7 y - p\gamma_6 A_0\cos(\Omega\tau)\right], \\
\dot{z} = \dfrac{1}{\gamma_2}\left[(\gamma_1+\gamma_5+\gamma_8)x - \gamma_8 y + \left(\dfrac{\gamma_5}{\gamma_4} - \dfrac{\gamma_2}{\gamma_0}\right)z - \left(\dfrac{\gamma_5}{\gamma_4} + \dfrac{\gamma_2}{\gamma_3}\right)p\sinh(x) - p\gamma_5 A_0\cos(\Omega\tau)\right]
\end{cases} \tag{6}
$$

where by the dots, we mean the differentiation with respect to the dimensionless time τ, and where we have introduced the following dimensionless variables:

$$
x = \frac{V_d}{V_{ref}}, \quad y = \frac{V_{C1}}{V_{ref}}, \quad z = \frac{\rho i_L}{V_{ref}}, \quad V_{ref} = \eta V_{T,} \quad t = \tau\sqrt{LC} \tag{7}
$$

and parameters:

$$
\varepsilon = \frac{C}{C_1},\ \rho = \sqrt{\frac{L}{C}},\ p = \frac{2\rho I_s}{V_{ref}},\ \gamma_0 = \frac{\rho}{R},\ \gamma_i = \frac{\rho}{R_i},\ (i = 1, \ldots, 8), \quad A_0 = \frac{V_0}{2\rho I_s},\ \Omega = \frac{\omega 1}{\sqrt{LC}} \tag{8}
$$

Equation (6) can be rearranged to give the following form of forced Jerk differential equation:

$$
\left(1 + \frac{p}{\gamma_3}\cosh(x)\right)\dddot{x} + \left[a_0\left(1 + \frac{p}{\gamma_3}\cosh(x)\right) + p\cosh(x) + \frac{3p}{\gamma_3}\dot{x}\sinh(x)\right]\ddot{x} + \left[-b_0 + \left(c_0 + \frac{1}{\gamma_3}\dot{x}^2\right)p\cosh(x) + d_0\left(1 + \frac{p}{\gamma_3}\cosh(x)\right) + d_1\dot{x}\sinh(x)\right]\dot{x} - d_2 x + a_1 p\sinh(x)
$$
$$
= \left(\varepsilon_1\Omega + \Omega^3\right)pA_0\sin(\Omega\tau) + \left(\varepsilon_2 + \varepsilon_3\Omega^2\right)pA_0\cos(\Omega\tau) \tag{9}
$$

with

$$
a_0 = \varepsilon\gamma_7 + \frac{1}{\gamma_0} - \frac{\gamma_5}{\gamma_2\gamma_4},\ a_1 = \varepsilon\gamma_7\left(\frac{1}{\gamma_6} + \frac{1}{\gamma_3}\right),\ b_0 = \frac{\gamma_1+\gamma_5+\gamma_6}{\gamma_2},
$$
$$
c_0 = -1 + \frac{1}{\gamma_0} + \frac{1}{\gamma_3},\ d_0 = \frac{1+\varepsilon\gamma_8\gamma_6}{\gamma_4\gamma_2} - \frac{1}{\gamma_0},
$$
$$
d_1 = \left(\frac{1}{\gamma_0} - \frac{\gamma_5}{\gamma_2\gamma_4}\right)\frac{1}{\gamma_3} + 1 + \frac{\varepsilon\gamma_7}{\gamma_3},\ d_2 = \frac{\varepsilon\gamma_7}{\gamma_2}(\gamma_1+\gamma_5+\gamma_8),
$$
$$
\varepsilon_1 = \frac{\gamma_5}{\gamma_2} - \frac{\varepsilon\gamma_8\gamma_6}{\gamma_4\gamma_2} - \frac{\varepsilon\gamma_7}{\gamma_0} + \frac{\varepsilon\gamma_5\gamma_7}{\gamma_4\gamma_2},
$$
$$
\varepsilon_2 = \frac{\gamma_5}{\gamma_2} + \frac{\varepsilon\gamma_8\gamma_6}{\gamma_2},\ \varepsilon_3 = \frac{\gamma_5}{\gamma_2\gamma_4} - \frac{1}{\gamma_0} + 1, \tag{10}
$$

where

$$
z = p\sinh(x) + pA_0\Omega\sin(\Omega\tau) + \dot{x}\left(1 + \frac{p}{\gamma_3}\cosh(x)\right) \tag{11}
$$

$$
y = \frac{1}{\gamma_8}\Bigg\{(\gamma_1+\gamma_5+\gamma_8)x - \gamma_2\left(\frac{1}{\gamma_0} + \frac{1}{\gamma_3}\left(1 + \dot{x}^2\right)\right)p\sinh(x) + \left(\left(\frac{\gamma_5}{\gamma_4} - \frac{\gamma_2}{\gamma_0}\right)\dot{x} - \gamma_2\ddot{x}\right)\left(1 + \frac{p}{\gamma_3}\cosh(x)\right) - p\gamma_2\dot{x}\cosh(x) - \left(\gamma_5 + \gamma_2\Omega^2\right)pA_0\cos(\Omega\tau) + \left(\frac{\gamma_5}{\gamma_4} - \frac{\gamma_2}{\gamma_0}\right)pA_0\Omega\sin(\Omega\tau)\Bigg\} \tag{12}
$$

It is obvious that the set of Eq.(6) is invariant under the transformation: $(x;y;z,\tau) \Leftrightarrow (-x;-y;-z,\tau+\pi/\Omega)$. Therefore, if $(x(\tau);y(\tau);z(\tau))$ is a solution of the set of Eq.(6) for a special set of parameters, then $(-x(\tau+\pi/\Omega);-y(\tau+\pi/\Omega);-z(\tau+\pi/\Omega))$ is also a solution for the same parameters set.

III. Analytical Analysis of the System's Dynamics

3.1 Equilibrium Points

The set of Eq. (6) can be seen as the forced Jerk equation, used to model the forced Tamasevicius circuit given by Fig. 1. In contrast to the unforced cases, Eq.(6) is non-autonomous, that is, time τ explicitly appears in the equation in the $\cos(\Omega\tau)$ and $\sin(\Omega\tau)$ terms. The phase plane is no longer a suitable arena in which to investigate this equation since the vector field at a given point changes in time, allowing a trajectory to return to that point and intersect itself. The system may be made autonomous, however, by increasing its dimension by one as follows:

$$
\begin{cases}
\dot{x} = \left(z - p\sinh(x) - pA_0\Omega\sin(\varphi)\right) / \left(1 + \dfrac{p}{\gamma_3}\cosh(x)\right), \\
\dot{y} = \varepsilon\left[\dfrac{\gamma_6}{\gamma_4}\left(z - p\sinh(x)\right) - \gamma_7 y - p\gamma_6 A_0\cos(\varphi)\right], \\
\dot{z} = \left[(\gamma_1+\gamma_5+\gamma_8)x - \gamma_8 y + \left(\dfrac{\gamma_5}{\gamma_4} - \dfrac{\gamma_2}{\gamma_0}\right)z - \left(\dfrac{\gamma_5}{\gamma_4} + \dfrac{\gamma_2}{\gamma_3}\right)p\sinh(x) - p\gamma_5 A_0\cos(\varphi)\right], \\
\dot{\varphi} = \Omega,
\end{cases} \tag{13}
$$

with $\varphi = \Omega\tau$. This system of four first order ordinary differential equation is defined on a phase space with topology $R^3 \times S$, where the circle S comes from the fact that the vector field of (13) is 2π-periodic in φ. A convenient scheme for viewing this four-dimensional flow in three dimensions is by way of a Poincare map M. This map is generated by the flow's intersection with a surface of section Σ which may be taken as Σ: φ = 0 (mod 2π). The Poincare map M : Σ → Σ is defined as follows: Let *P* be a point on Σ, and using it as an initial condition for the flow (13), let the resulting trajectory evolves in time until φ = 2π, that is until it once again intersects Σ, this time at some point *Q*. Then M maps *P* to *Q*. Note that a fixed point of the Poincare map corresponds to a 2π-periodic motion of the flow. Solving then the system equation (13) $(\dot{x} = \dot{y} = \dot{z} = 0)$ for φ = 0 (mod 2π) leads the following solutions which is the equilibrium point (x_0, y_0, z_0) of the system given by:

$$
x_0 = \lambda,\ y_0 = -\frac{\gamma_6}{\gamma_7}pA_0,\ z_0 = p\sinh(\lambda), \tag{14}
$$

where λ is the solution of the following equation:

$$
(\gamma_1+\gamma_5+\gamma_8)\lambda - \left(\frac{\gamma_2}{\gamma_0} + \frac{\gamma_2}{\gamma_3}\right)p\sinh(\lambda) + pA_0\left(\frac{\gamma_6\gamma_8}{\gamma_7} - \gamma_5\right) = 0 \tag{15}
$$

From where it appears that when $\sigma < 1$ with $\sigma = \gamma_0\gamma_3(\gamma_1+\gamma_5+\gamma_8)/p\gamma_2(\gamma_0+\gamma_3)$ Eq.(15) admits only one solution and as a consequence, the system admits one equilibrium point:

However, if σ>1 one has by setting:

$$
F = p^2A_0^2\left(\frac{\gamma_6\gamma_8}{\gamma_7} - \gamma_5\right)^2 - \left[(\gamma_1+\gamma_5+\gamma_8)\operatorname{arcosh}(\sigma) - \left(\frac{\gamma_2}{\gamma_0} + \frac{\gamma_2}{\gamma_3}\right)p\sqrt{\sigma^2 - 1}\right]^2 \tag{16}
$$

The following set of situations:

- If F < 0, then Eq. (15) admits three solutions (as illustrated by Fig. 3), and then three equilibrium points.
- Otherwise, that is when $F > 0$ Eq. (15) admits only one equilibrium point.

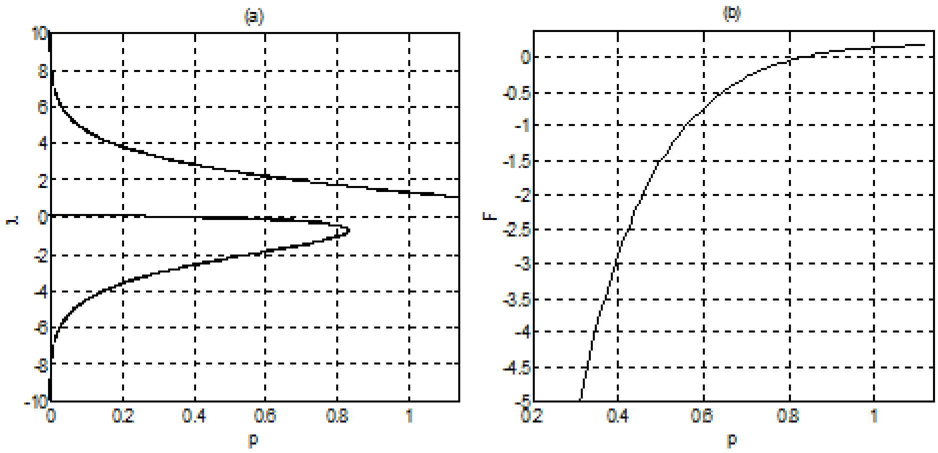

Fig. 2. (a) Solution of Eq. (15), (b) plot of F given by (16), for the varying value of parameter p, and for the parameters chosen as: $\gamma_0 = \gamma_1 = \gamma_2 = \gamma_3 = 4, \gamma_5 = \gamma_7 = \gamma_8 = 1$, and $A_0 = 0.5$ It is obvious that this equation admits three solutions for F<0 and only one for F>0.

3.2 Stability of Equilibrium Points.

Physically, a steady state solution corresponds to an equilibrium state of the system and the behavior of the system may depend on its stability. To test this stability for $\varphi = 0(mod\, 2\pi)$, let us consider the state $E = E_0 + \delta E$ vector, where $E \equiv E(x, y, z)$ and $\delta E(x_1, y_1, z_1)$ is the perturbation of the equilibrium solution $E_0(x_0, y_0, z_0)$. Thus we obtain the following system equation:

$$\begin{cases} \dot{x}_1 = \dfrac{1}{1+\dfrac{p}{\gamma_3}\cosh(\lambda)}\left[-p\cosh(\lambda)x_1 + z_1\right], \\ \dot{y}_1 = \varepsilon\left[-\dfrac{\gamma_6}{\gamma_4}p\cosh(\lambda)x_1 - \gamma_7 y_1 + \dfrac{\gamma_6}{\gamma_4}z_1\right], \\ \dot{z} = \dfrac{1}{\gamma_2}\left[\begin{array}{c}(\gamma_1+\gamma_5+\gamma_8 - \left(\dfrac{\gamma_5}{\gamma_4}+\dfrac{\gamma_2}{\gamma_3}\right)p\cosh(\lambda))x_1 \\ -\gamma_8 y_1 + \left(\dfrac{\gamma_5}{\gamma_4}-\dfrac{\gamma_2}{\gamma_0}\right)z_1\end{array}\right], \end{cases} \tag{17}$$

which leads to the following 3× 3 Jacobean matrix:

$$\begin{bmatrix} -p\cosh(\lambda)/\left(1+\dfrac{p}{\gamma_3}\cosh(\lambda)\right) & 0 & 1/\left(1+\dfrac{p}{\gamma_3}\cosh(\lambda)\right) \\ -\varepsilon p\dfrac{\gamma_6}{\gamma_4}\cosh(\lambda) & -\gamma_7\varepsilon & \varepsilon(\gamma_6/\gamma_4) \\ \dfrac{1}{\gamma_2}\left[(\gamma_1+\gamma_5+\gamma_8 - p\left(\dfrac{\gamma_5}{\gamma_4}+\dfrac{\gamma_2}{\gamma_3}\right)\cosh(\lambda)\right] & -\dfrac{\gamma_8}{\gamma_2} & \dfrac{1}{\gamma_2}\left(\dfrac{\gamma_5}{\gamma_4}-\dfrac{\gamma_2}{\gamma_0}\right) \end{bmatrix} \tag{18}$$

Thus the Jacobean matrix evaluated at the equilibrium point E_0 satisfies the following characteristic equation:

$$\lambda^3 + P_0\lambda^2 + P_1\lambda + P_2 = 0 \tag{19}$$

with:

$$P_0 = \varepsilon\gamma_4 - \frac{1}{\gamma_2}\left(\frac{\gamma_5}{\gamma_4}-\frac{\gamma_2}{\gamma_0}\right) + \frac{p\cosh(\lambda)}{1+\dfrac{p}{\gamma_3}\cosh(\lambda)}$$

$$P_1 = \frac{1}{1+\dfrac{p}{\gamma_3}\cosh(\lambda)}\left[\left(\varepsilon\gamma_7 + \frac{1}{\gamma_0}+\frac{1}{\gamma_3}\right)p\cosh(\lambda) - \frac{(\gamma_1+\gamma_5+\gamma_8)}{\gamma_2}\right] + \frac{\varepsilon}{\gamma_2}\left[\frac{\gamma_6\gamma_8}{\gamma_4} - \gamma_7\left(\frac{\gamma_5}{\gamma_4}-\frac{\gamma_2}{\gamma_0}\right)\right]$$

$$P_2 = \frac{\varepsilon\gamma_7}{\gamma_2\left(1+\dfrac{p}{\gamma_3}\cosh(\lambda)\right)}\left[\left(\frac{-2\gamma_5}{\gamma_4}+\frac{\gamma_2}{\gamma_0}-\frac{\gamma_2}{\gamma_3}\right)p\cosh(\lambda) + \gamma_1+\gamma_5+\gamma_8\right] \tag{20}$$

According to the Routh-Hurwitz criterion, all roots of Eq.(19) would have negative real parts if the following constraints are satisfied $P_0 > 0, P_1 > 0, P_2 > 0$, and $P_0P_1 - P_2 > 0$. These criteria are plotted in Fig.(4) for parameters chosen as in Fig.(3), from where it appears that all these parameters are positive for p belonging to interval [0.161, 1.14], leading each equilibrium point $E(x_0, y_0, z_0)$ to be stable saddle focus. Physically, this result supports the fact that the oscillator can oscillate chaotically and admits the existence of stable fixed point motion in the system.

3.3 Weak Amplitude Oscillations in the System.

In order to approximate the solution of the system governed by Eq.(6), let us consider the ordinary differential Eq.(9), in which the following change of variables is taking into account: $d_2 = \epsilon\sigma_1 - a_0$, $b_0 = d_0 - 1 - \epsilon\sigma_2$, $p = \epsilon P$, $d_1 = \epsilon D_1$,, which leads Eq.(8) to:

International Journal of Scientific Engineering and Science
Volume 2, Issue 4, pp. 63-73, 2018. ISSN (Online): 2456-7361

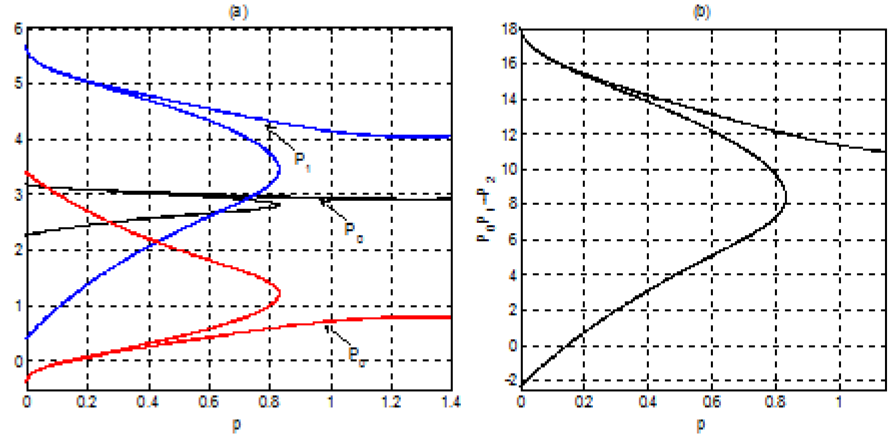

Fig. 4. (a) Parameters of the characteristic equation, (b) Plot of $P_0P_1-P_2$, for the varying value of parameter *p*, and for the parameters chosen in Fig. (3).

$$\left(1+\frac{p}{\gamma_3}\cosh(x)\right)\dddot{x}+\left[a_0\left(1+\frac{\epsilon P}{\gamma_3}\cosh(x)\right)+\epsilon P\cosh(x)+\frac{3\epsilon P}{\gamma_3}\dot{x}\sinh(x)\right]\ddot{x}+$$
$$\left[1+\epsilon\sigma_2+\left(c_0+\frac{1}{\gamma_3}\dot{x}^2\right)\epsilon P\cosh(x)+\frac{\epsilon P}{\gamma_3}\cosh(x)+\epsilon D_1\dot{x}\sinh(x)\right]\dot{x}+ \tag{21}$$
$$(a_0-\epsilon\sigma_1)x+a_1\epsilon P\sinh(x)=\epsilon P\left(\varepsilon_1\Omega+\Omega^3\right)A_0\sin(\Omega\tau)+$$
$$\epsilon P\left(\varepsilon_2+\varepsilon_3\Omega^2\right)A_0\cos(\Omega\tau)$$

In the follow, we use a perturbation method to investigate the dynamics of Eq.(21) for small values of ϵ. The idea of the method is that the expected form of solution involves two time scales: the fast time scale of the periodic motion itself $\xi=\Omega\tau$, and a slower time scale which represents the approach to the periodic motion $\eta=\epsilon\tau$. In order to substitute these definitions into the forced Eq. (21), we need expressions for the first, second and third derivatives of x with respect to τ. We obtain these by using the chain rule:

$$\frac{dx}{d\tau}=\frac{\partial}{\partial\xi}\frac{\partial\xi}{\partial\tau}+\frac{\partial}{\partial\eta}\frac{\partial\eta}{\partial\tau}=\Omega\frac{\partial}{\partial\xi}+\epsilon\frac{\partial}{\partial\eta},\quad \frac{d^2}{d\tau^2}=\Omega^2\frac{\partial^2}{\partial\xi^2}+2\epsilon\Omega\frac{\partial^2}{\partial\xi\partial\eta}+\ldots,$$
$$\frac{d^3}{d\tau^3}=\Omega^3\frac{\partial^3}{\partial\xi^3}+3\epsilon\Omega\frac{\partial^3}{\partial\xi^2\partial\eta}+\ldots, \tag{22}$$

Substituting (22) into (21) gives the following partial differential equation:

$$\left(1+\frac{\epsilon P}{\gamma_3}\cosh(x)\right)\left(\Omega^3\frac{\partial^3x}{\partial\xi^3}+3\epsilon\Omega\frac{\partial^3x}{\partial\xi^2\partial\eta}\right)+\left[a_0\left(1+\frac{\epsilon P}{\gamma_3}\cosh(x)\right)+\epsilon P\cosh(x)\right.$$
$$\left.+\frac{3\epsilon\Omega P}{\gamma_3}\frac{\partial x}{\partial\xi}\sinh(x)\right]\left(\Omega^2\frac{\partial^2x}{\partial\xi^2}+2\epsilon\Omega\frac{\partial^2x}{\partial\xi\partial\eta}\right)+\left[1+\epsilon\sigma_2+\left(c_0+\frac{\Omega^2}{\gamma_3}\left(\frac{\partial x}{\partial\xi}\right)^2\right)\epsilon P\cosh(x)+\right.$$
$$\left.\frac{\epsilon P}{\gamma_3}\cosh(x)+\epsilon D_1\frac{\partial x}{\partial\xi}\sinh(x)\right]\left(\Omega\frac{\partial x}{\partial\xi}+\epsilon\frac{\partial x}{\partial\eta}\right)+(a_0-\epsilon\sigma_1)x+a_1\epsilon P\sinh(x)$$
$$=\epsilon P\left(\varepsilon_1\Omega+\Omega^3\right)A_0\sin(\xi)+\epsilon P\left(\varepsilon_2+\varepsilon_3\Omega^2\right)A_0\cos(\xi) \tag{23}$$

Next we expand x and **Ω** in power series:

$$x=x_0+\epsilon x_1+\ldots,\ \Omega=1+\epsilon k_1+\ldots \tag{24}$$

Substituting (24) into (23) and neglecting terms of $O(\epsilon^2)$, gives, after collecting terms:

- At order ϵ^0, one has

$$\frac{\partial^3x_0}{\partial\xi^3}+a_0\frac{\partial^2x_0}{\partial\xi^2}+\frac{\partial x_0}{\partial\xi}+a_0x_0=0, \tag{25}$$

- However, the order ϵ^1 yields:

$$\frac{\partial^3x_1}{\partial\xi^3}+a_0\frac{\partial^2x_1}{\partial\xi^2}+\frac{\partial x_1}{\partial\xi}+a_0x_1=-\left\{\left(3k_1+\frac{P}{\gamma_3}\cosh(x_0)\right)\frac{\partial^3x_0}{\partial\xi^3}+3\frac{\partial^3x_0}{\partial\xi^2\partial\eta}+\right.$$
$$\left(2k_1a_0+\left(1+\frac{a_0}{\gamma_3}\right)P\cosh(x_0)+\frac{3P}{\gamma_3}\frac{\partial x_0}{\partial\xi}\sinh(x_0)\right)\frac{\partial^2x_0}{\partial\xi^2}+$$
$$2a_0\frac{\partial^2x_0}{\partial\xi\partial\eta}+\left[k_1+\sigma_2+\left(c_0+\frac{d_0P}{\gamma_3}+\frac{P}{\gamma_3}\left(\frac{\partial x_0}{\partial\xi}\right)^2\right)\cosh(x_0)+D_1\frac{\partial x_0}{\partial\xi}\sinh(x_0)\right]\frac{\partial x_0}{\partial\xi}$$
$$\left.+\frac{\partial x_0}{\partial\eta}-\sigma_1x_0+a_1P\sinh(x_0)\right\}+P(\varepsilon_1+1)A_0\sin(\xi)+$$
$$P(\varepsilon_2+\varepsilon_3)A_0\cos(\xi) \tag{26}$$

Equation (25) admits the general solution in the form:

$$x_0(\xi,\eta)=A(\eta)\exp(-a_0\xi)+B(\eta)\cos(\xi)+C(\eta)\sin(\xi) \tag{27}$$

Note here that the constants of integration A, B and C are in fact arbitrary functions of slow time η since (23) is a partial differential equation. Substituting (27) into (26) we obtain an equation containing resonant terms (that is terms proportional to $\exp(-a_0\xi)$, $\cos(\xi)$ and $\sin(\xi)$ and also non resonant terms. We require the coefficients of resonant terms to vanish, the well-known secularity condition, giving the following slow flow:

$$\left(1+a_0^2\right)\frac{\partial A}{\partial\eta}-A\left[P\left(\frac{a_0^2}{\gamma_3}\left(a_0-P-\gamma_3+\frac{d_0}{a_0}\right)-a_1\right)+\sigma_1+a_0\left(c_0+\sigma_2+k_1\left(1+a_0^2\right)\right)+\right.$$
$$\frac{1}{2}\left(B^2+C^2\right)\frac{P^2}{\gamma_3}\left(1-\frac{a_0^2}{2}\right)-D_1+a_0\left(\frac{c_0}{2}+\frac{3}{\gamma_3}\right)+$$
$$\left.P\left(1-\frac{a_1}{2}-\frac{a_0^2}{2}-\frac{3a_0}{\gamma_3}+\frac{a_0^3}{2\gamma_3}+\frac{a_0d_0}{2\gamma_3}\right)\right]=0 \tag{28}$$

$$2a_0\frac{\partial B}{\partial\eta}+2\frac{\partial C}{\partial\eta}+B\left[\frac{1}{8}\left(c_0+\frac{P(d_0-7)+6}{\gamma_3}\right)\left(B^2+C^2\right)+\frac{P}{\gamma_3}(d_0-1)+c_0-2k_1+\sigma_2\right]+$$
$$C\left[\frac{1}{8}\left(-a_1P-2D_1+3P\left(1+\frac{P}{\gamma_3}\right)\right)\left(B^2+C^2\right)-a_1P+\right.$$
$$\left.\sigma_1+2a_0k_1+P\left(1+\frac{P}{\gamma_3}\right)\right]=-P(1+\varepsilon_1)A_0 \tag{29}$$

$$2\frac{\partial B}{\partial\eta}-2a_0\frac{\partial C}{\partial\eta}+B\left[\frac{1}{8}\left(-a_1P-2D_1+3P\left(1+\frac{P}{\gamma_3}\right)\right)\left(B^2+C^2\right)\right.$$
$$\left.-a_1P+\sigma_1+2a_0k_1+\left(1+\frac{P}{\gamma_3}\right)\right]-C\left[\frac{1}{8}\left(c_0+\frac{P(d_0-7)+6}{\gamma_3}\right)\left(B^2+C^2\right)+\frac{P}{\gamma_3}(d_0-1)\right.$$

International Journal of Scientific Engineering and Science
Volume 2, Issue 4, pp. 63-73, 2018. ISSN (Online): 2456-7361

$$+c_0 - 2k_1 + \sigma_2\big] = -\mathrm{P}(\varepsilon_2+\varepsilon_3)\mathrm{A}_0 \tag{30}$$

Equilibrium points of the slow flow (28-30) correspond to periodic motions of the forced Eq.(9), to be determined by setting $\frac{\partial A}{\partial \eta}, \frac{\partial B}{\partial \eta}, and \frac{\partial C}{\partial \eta}$ to zero. Equation (28) leads to the trivial solution $A=0$, while the set of equation (29) and (30) lead to the following solution:

$$B = -PA_0 \frac{\left((1+\varepsilon_1)\mathrm{S}_{11} + (\varepsilon_2+\varepsilon_3)\mathrm{S}_{21}\right)R^2 + (1+\varepsilon_1)\mathrm{S}_{12} + (\varepsilon_2+\varepsilon_3)\mathrm{S}_{22}}{\left(\mathrm{S}_{11}R^2+\mathrm{S}_{12}\right)^2 + \left(\mathrm{S}_{21}R^2+\mathrm{S}_{22}\right)^2}$$

$$C = PA_0 \frac{\left((\varepsilon_2+\varepsilon_3)\mathrm{S}_{11} - (1+\varepsilon_1)\mathrm{S}_{21}\right)R^2 + (\varepsilon_2+\varepsilon_3)\mathrm{S}_{12} - (1+\varepsilon_1)\mathrm{S}_{22}}{\left(\mathrm{S}_{11}R^2+\mathrm{S}_{12}\right)^2 + \left(\mathrm{S}_{21}R^2+\mathrm{S}_{22}\right)^2} \tag{31}$$

with

$$\mathrm{S}_{11} = \frac{1}{8}\left(c_0 + \frac{P(d_0-7)+6}{\gamma_3}\right),\ \mathrm{S}_{12} = \frac{P}{\gamma_3}(d_0-1) + c_0 - 2k_1 + \sigma_2\ ,$$

$$\mathrm{S}_{21} = \frac{1}{8}\left(-a_1P - 2D_1 + 3P\left(1+\frac{P}{\gamma_3}\right)\right),\ \mathrm{S}_{22} = -a_1P + \sigma_1 + 2a_0k_1 + P\left(1+\frac{P}{\gamma_3}\right) \tag{32}$$

where $R^2 = B^2 + C^2$. Squaring the top of (31) and adding it to the square of the bottom gives:

$$\left(S_{11}^2+S_{21}^2\right)^2 R^{10} + 4\left(S_{11}^2+S_{21}^2\right)\left(S_{11}S_{12}+S_{21}S_{22}\right)R^8 + \Big[2\left(S_{11}^2+3S_{21}^2\right)\left(S_{12}^2+S_{22}^2\right) +$$

$$8\,S_{11}S_{12}S_{21}S_{22}\Big]R^6 + \Big[4\left(S_{12}^2+S_{22}^2\right)\left(S_{11}S_{12}+S_{21}S_{22}\right) - P^2A_0^2\left(S_{11}^2+S_{21}^2\right)\left((1+\varepsilon_1)^2+(\varepsilon_2+\varepsilon_3)^2\right)\Big]R^4$$

$$+\Big[\left(S_{12}^2+S_{22}^2\right)^2 - 2PA_0\left(S_{11}S_{12}+S_{21}S_{22}\right)\left((1+\varepsilon_1)^2+(\varepsilon_2+\varepsilon_3)^2\right)\Big]\mathrm{R}^2 -$$

$$\left(S_{12}^2+S_{22}^2\right)\left((1+\varepsilon_1)^2+(\varepsilon_2+\varepsilon_3)^2\right) = 0 \tag{33}$$

This equation is solved numerically to give the result plotted in Figs. 5, 6 and 7, for the set of parameters: $\sigma_1 = 2\sigma_2 = 0.5$, $\gamma_3 = 0.6702$, $a_0 = 5.6109,$ $c_0 = 1.4868,$ $d_0 = 4.9891,$ $k_1 = 0.4,$ $a_1 = 30.55,$ $D_1 = 0.05$. As one can see from these figures, Eq.(33) admits one or three real solutions according to the chosen values of P, A_0 and γ_2. From (26) and (31), the stationary periodic solution of Eq.(9) can be approximated as:

$$\mathrm{x}(\tau) = \mathrm{PA}_0\left[\frac{\left((\varepsilon_2+\varepsilon_3)\mathrm{S}_{11} - (1+\varepsilon_1)\mathrm{S}_{21}\right)\mathrm{R}^2 + (\varepsilon_2+\varepsilon_3)\mathrm{S}_{12} - (1+\varepsilon_1)\mathrm{S}_{22}}{\left(\mathrm{S}_{11}\mathrm{R}^2+\mathrm{S}_{12}\right)^2 + \left(\mathrm{S}_{21}\mathrm{R}^2+\mathrm{S}_{22}\right)^2}\sin(\Omega\tau)\right.$$

$$\left. - \frac{\left((1+\varepsilon_1)\mathrm{S}_{11} + (\varepsilon_2+\varepsilon_3)\mathrm{S}_{21}\right)\mathrm{R}^2 + (1+\varepsilon_1)\mathrm{S}_{12} + (\varepsilon_2+\varepsilon_3)\mathrm{S}_{22}}{\left(\mathrm{S}_{11}\mathrm{R}^2+\mathrm{S}_{12}\right)^2 + \left(\mathrm{S}_{21}\mathrm{R}^2+\mathrm{S}_{22}\right)^2}\cos(\Omega\tau)\right] \tag{34}$$

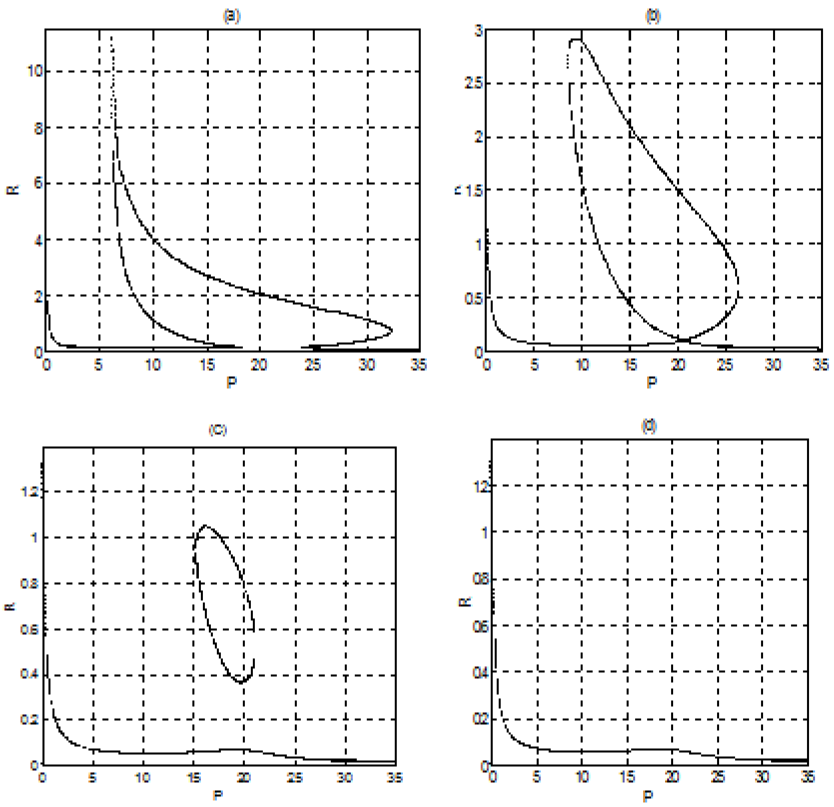

Fig. 5. Amplitude $R = \sqrt{B^2 + C^2}$ obtained by solving the polynomial Eq. (33) for varying values of P and for: (a): $A_0 = 10,$ (b): $A_0 = 5$, (c): $A_0 = 2$, and (d): $A_0 = 0.5$.

International Journal of Scientific Engineering and Science
Volume 2, Issue 4, pp. 63-73, 2018. ISSN (Online): 2456-7361

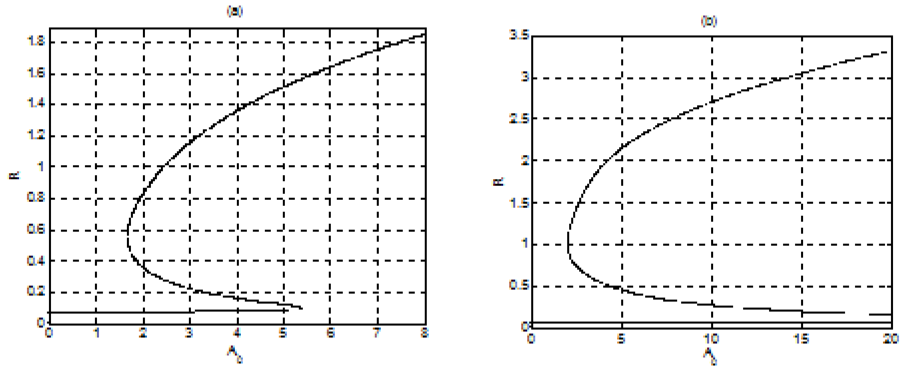

Fig. 6. Amplitude $R=\sqrt{B^2+C^2}$ obtained by solving the polynomial Eq. (33) for varying values of A_0 and for: (a): $P=20$, and (b): $P=15$.

From these obvious results, it appears that the dynamics of the oscillator studied in the present paper may be improved by an appropriate choice of the nonlinearity coefficient p, introduced by the pair of nonlinear diodes, the amplitude A_0 of the driven signal voltage and the tuning parameter γ_2.

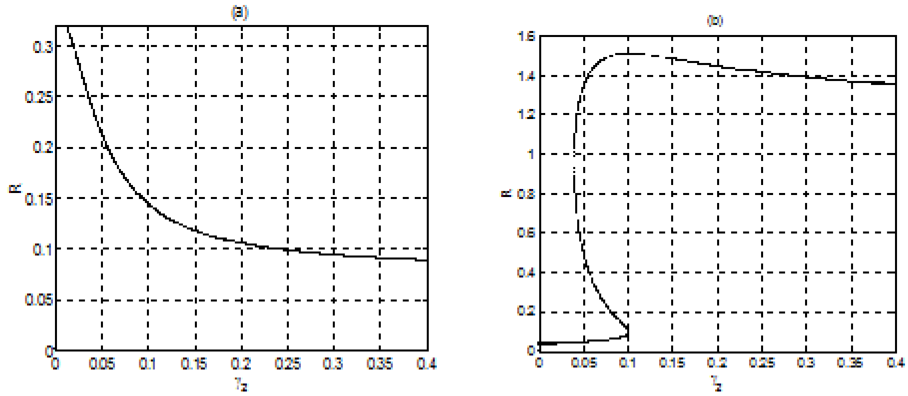

Fig. 7. Amplitude $R=\sqrt{B^2+C^2}$ obtained by solving the polynomial Eq. (33) for varying values of γ_2 and for $A_0=5$: (a): $P=2$, and (b): $P=20$.

IV. Numerical Study

4.1. Preliminary: Numerical Methods.

To explore the dynamics of the oscillator studied in present paper, the system Eq.(6) is numerically integrated using the differential transform method [14], with the time grid always kept, $\Delta\tau=0.001$. The computations were performed out using the values of electronic components given in (3), which leads to the following parameters values:

$$\gamma_1=6.7020.10^{-3},\ \gamma_3=6.7020.10^{-3}, \gamma_4=0.245, \gamma_5=2.6808.10^{-3}$$
$$\gamma_6=\gamma_7=2.0106.10^{-2},\quad \gamma_8=1.0053.10^{-2},\ \gamma_0=10.0530,\quad p=2.18.10^{-5}$$
$$\rho=201.0610,\ \varepsilon=40, \tag{35}$$

while γ_2 and γ_4 are chosen as the tuning parameters. For each set of parameters, the set of Eq.(6) is integrated for a sufficiently long time and the transient is discarded. Various bifurcation diagrams, combined with the corresponding graphs of the maximum Lyapunov exponent are plotted to define the type of transition leading to chaos in the system. The bifurcation diagrams are obtained by plotting the local maxima of states variables in terms of the bifurcation control parameter γ_2. The Lyapunov exponent in this part helps to distinguish the regular oscillations characterized by the negative exponent and chaotic behaviors marked by the positive ones.

4.2. Routes to Chaos.

To investigate the sensitivity of the system with respect to a single parameter γ_2, we fix $\Omega=2.3$, $V_0=0.05$ and vary γ_2 in the range $0.01\le\gamma_2\le 2$. It appears when increasing γ_2 as illustrated in Fig.(8.a) that, the system undergoes a Hopf bifurcation giving rise to a stable period-1 limit cycle. Further increasing γ_2, this period-1 limit cycle converts to a chaotic band attractor via a period doubling bifurcation. The graph of maximum Lyapunov exponents is depicted in Fig.(8.b) which shows a very good coincidence with the bifurcation one. In particular, bands of chaos characterized by positive values the maximum Lyapunov exponents can easily be identified in these graphs.

It is obvious as evidence in Figs. (9-11) that the oscillator studied here is also sensitive to the parameter γ_4. These figures which show new phenomena such as the bubbles bifurcation (as shown in Figs. (9) and (10)) leading to chaotic behaviors (see Fig.(11)).

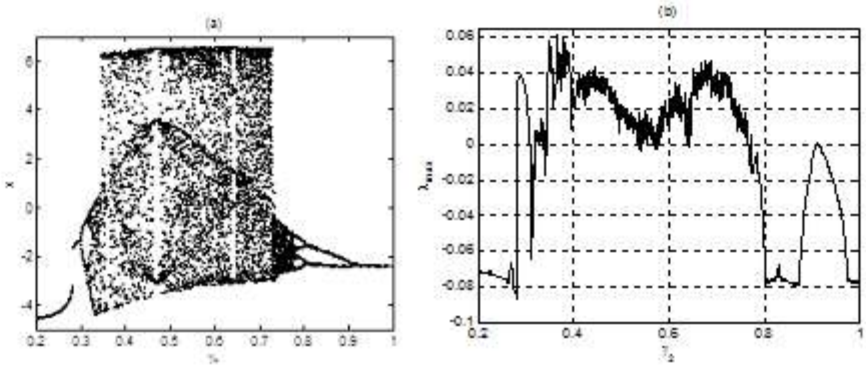

Fig. 8. (a) Bifurcation diagram, and (b) corresponding Lyapunov exponent, obtained by using the values of parameters (35), with $\gamma_4 = 1.1$.

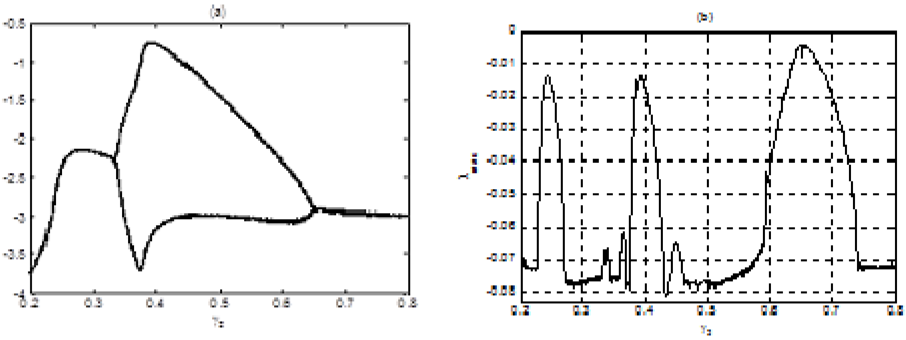

Fig. 9. (a) Bifurcation diagram in the form of Bubble, and (b) corresponding Lyapunov exponent, obtained by using the values of parameters (35), with $\gamma_4 = 0.82$.

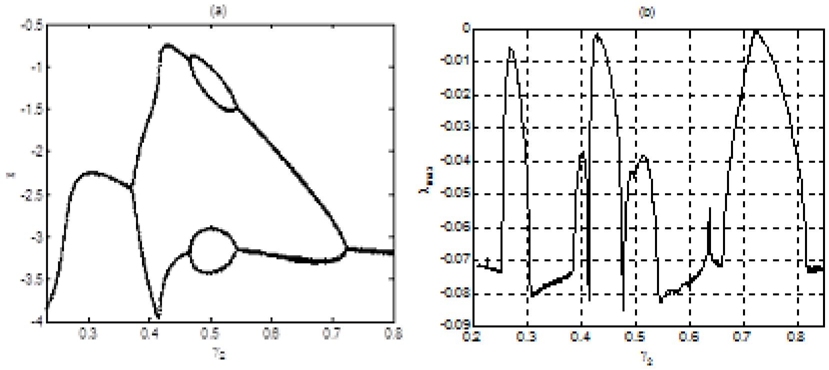

Fig. 10. (a) Bifurcation diagram in the form Bubble, obtained by using the values of parameters (35), with $\gamma_4 = 0.84$, showing the periodic doubling of that given in Fig.(9), and (b) corresponding Lyapunov exponent

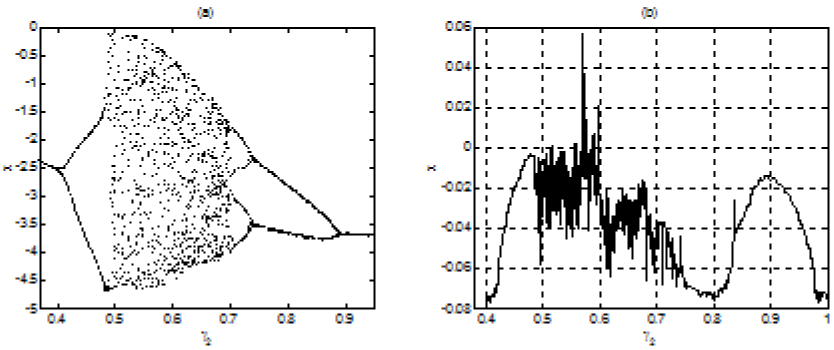

Fig. 11. (a) Bifurcation diagram, and (b) corresponding Lyapunov exponent, obtained by using the values of parameters (35), with $\gamma_4 = 1.8$. The chaotic windows can easily be seen.

International Journal of Scientific Engineering and Science
Volume 2, Issue 4, pp. 63-73, 2018. ISSN (Online): 2456-7361

4.3. Others Behavior of System: Generation of Train of Regular and Chaotic Pulses.

To prove the validity of the present studies and that the forced oscillator depicted in Fig.1 can generate chaotic pulses, the sample phase portraits shown in Fig.12d, with corresponding time traces in Fig.12a, and computed for $\gamma_2 = 0.55$ and $\gamma_4 = 1.1$, shows three equilibrium points and trajectories starting at the equilibrium point zero and end at the same equilibrium point, the well-known homoclinic orbit corresponding to pulse signal. As $\gamma_2 = 0.55$ belong to chaotic window, the corresponding signals generated here are chaotic like pulses. Next, by choosing the tuning parameters in regular band as sketched in Figs.(13-15), one obtains the generation of regular pulses and impulses signals.

V. Pspice Simulations and Experimental Studies

5.1. Pspice simulations.

Circuit simulation packages such as Pspice have become adequate tools for dynamical simulation of nonlinear circuits. Taking full advantage of this simulation software, we have made simulations with the aim of confirmation of the validity numerical approach. Based on the theoretical analysis presented above, realistic Pspice simulations of the system shown in fig. 1 are simulated, in order to validate the mathematical model proposed in this work. With a worry to generate trains of regular and chaotic pulses, several simulations are made. Thus, Figs. 12-b and 13.b expresses the chaotic behavior of the system, while Figs. 14-b, 15-b and 16-b show the time dependent signal voltage, leading to the generation of regular pulses, agreeing the results of numerical investigations. By conveniently choosing the values of the components, one can also have the scenario of impulse generation (identical to modulated signals), as shown in Fig.(16).

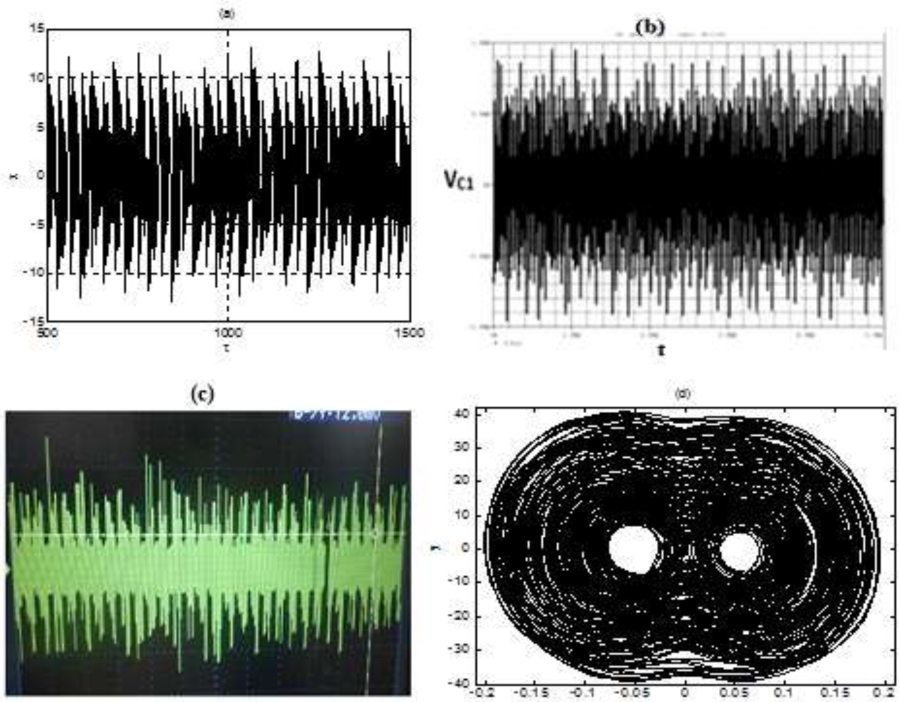

Fig. 12. Time dependent signal voltage obtained (a) numerically, (b) by pspice simulation, and (c) experimentally. While (d) is the phase space trajectory in (x - y) plane, obtained numerically for $R_2 = 360\Omega$, leading to $\gamma_2 = 0.55$ and $\gamma_4 = 1.1$.

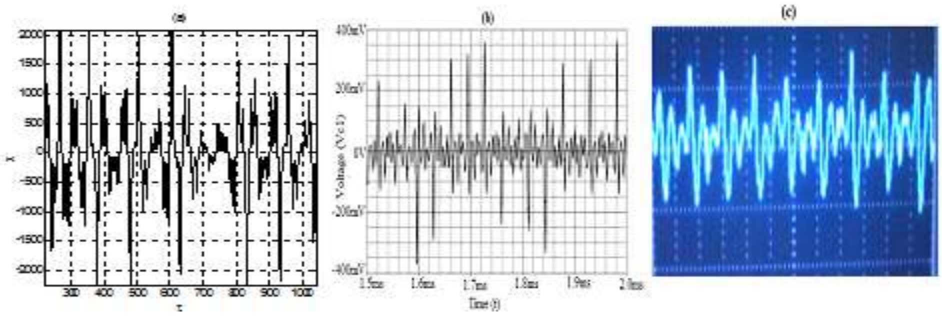

Fig. 13. Time dependent signal voltage obtained: (a) numerically (b) by Pspice simulation, (c) experimentally and with $R_2 = 1.5k\Omega$, leading to $\gamma_2 = 0.13$ and $\gamma_4 = 0.11$. As on can see, the system exhibits chaotic pulse like behavior.

Volume 2, Issue 4, pp. 63-73, 2018. ISSN (Online): 2456-7361

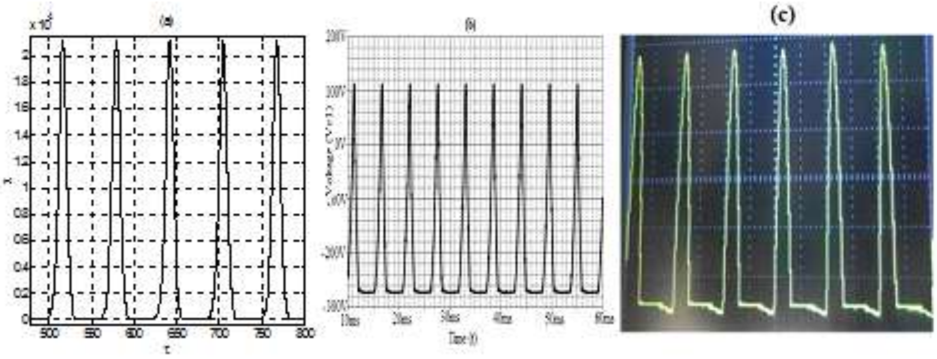

Fig. 14. Time dependent signal voltage obtained: (a) numerically (b) by Pspice simulation, (c) experimentally and with $R_2 = 6k\Omega$, leading to $\gamma_2 = 0.03$ and $\gamma_4 = 1.5$. As on can see, the system exhibits regular pulse like behavior.

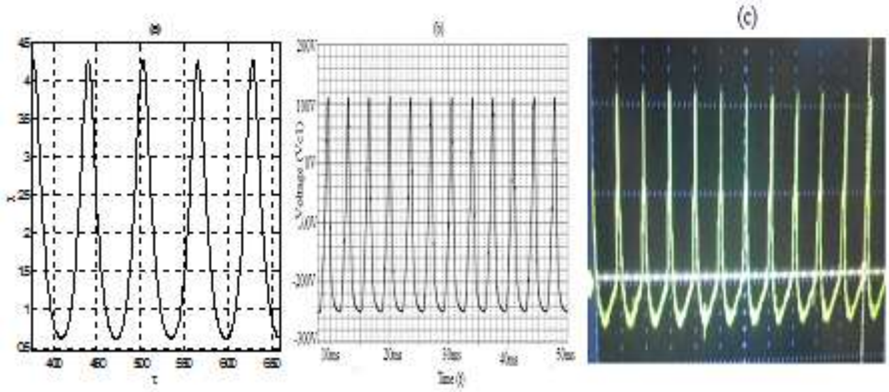

Fig. 15. Time dependent signal voltage obtained: (a) numerically (b) by Pspice simulation, (c) experimentally and with $R_2 = 7.5k\Omega$, leading to $\gamma_2 = 0.02$ and $\gamma_4 = 0.92$. As on can see, the system exhibits regular pulse like behavior.

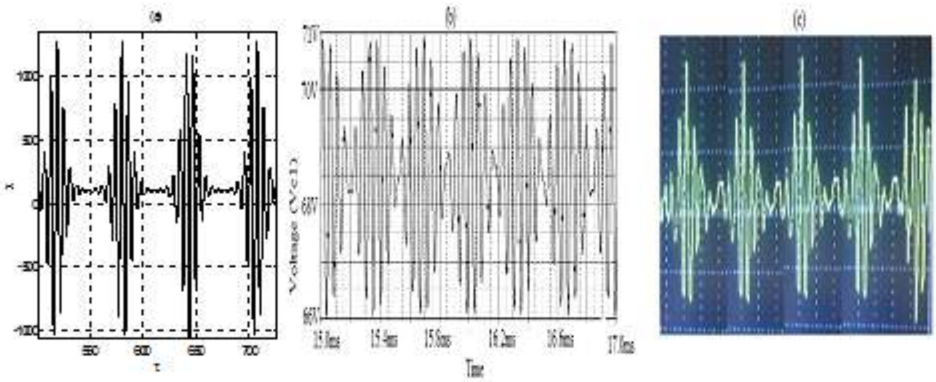

Fig. 16. (a) Time dependent signal voltage obtained: (a) numerically (b) by Pspice simulation, (c) experimentally and with $R_2 = 1.3k\Omega$, leading to $\gamma_2 = 0.15$ and $\gamma_4 = 1.6$. As on can see, the system exhibits regular impulses like behavior.

5.2 Experimental checking.

The photograph of the circuit used in our experiments is illustrated in Fig. (2). The experimental results are obtained by observing as a function of time the voltages across the capacitor (C_1), As in the case of numerical and PSPICE simulations, the oscillator's dynamics changes substantially when the resistor R_2 is monitored. This is clearly demonstrated by the experimental results depicted in Figures (12.c) to (16.c), showing the real behavior of the oscillator under investigation in the present work. The experimental results were generally close to those obtained from the theoretical and numerical methods, and a very good qualitative agreement is obtained while comparing the experimental values of the control parameter R_2 with those of numerical and PSPICE simulations.

VI. Conclusion

In this paper, we have studied the possible generation of the pulse signals using an electrical circuit conveniently built,

Volume 2, Issue 4, pp. 63-73, 2018. *ISSN (Online): 2456-7361*

driven by a low frequency signal voltage generator. After deriving the set of nonlinear ordinary differential equations describing the dynamical behavior the model, we have used them to find the equilibrium points and next analyze their stabilities. By using the same set of equations, and via the two parameters approximation method, the analytical periodic solution have been approximated and proved to be sensitive to the variations of the nonlinearity coefficient and the amplitude of the driven signal voltage. Next in the first intention to confirm the validity of our analytical findings, numerical investigations were performed, showing new behaviors, not observed analytically, namely the system bifurcation and its evolution to chaos as well as the bubble bifurcation which does not reach to chaos, obtained just by varying the value of the resistor R_2 chosen as the tuning component. This choice being attributed to the fact that nonlinear diode parameter is not easily tunable experimentally. For certain values of parameters, some special kind of signals in the form of pulses and impulses, useful in communication for signal process had been generated, which was evidenced through the phase space plot showing trajectories that start and end at the same fixed point, the well-known homoclinic orbits. Next, Pspice simulations as well as real experiments have been used to confirm both analytical and numerical results, and the obtained results appeared to be in good agreement for all investigations. In our future works, we will explore in detail a possible application of the circuit to synchronization and secured communication.

REFERENCES

[1] G. P. Agrawal, *Nonlinear Fiber Optics*, 2nd ed., Academic, New York, 1995.

[2] M. Remoissenet, *Waves Called Solitons*, 3rd ed., Springer-Verlag, Berlin, 1999.

[3] F. Kenmogne, David D. Yemélé, J. Kengne, D. Ndjanfang, "Transverse compactlike pulse signals in a two-dimensional nonlinear electrical network," *Physical Review E*, vol. 90, issue 5-1, 052921, 2014.

[4] H.-Y. Donkeng, F. Kenmogne, D. Yemélé, M. G. Jeutho, W. K. Mabou, D. NDjanfang, "Modulated compact-like pulse signals in a nonlinear electrical transmission line: A specific case studied," *Chinese Journal of Physics*, vol. 55, issue 3, pp. 683–691, 2017.

[5] F. Kenmogne, D. Yemélé, and P. Marquié, "Comment on "Dynamics and properties of waves in a modified Noguchi electrical transmission line" *Physical Review E*, vol. 94, issue 3-2, 036201, 2016.

[6] R. L. Filali, M. Benrejeb, and P. Borne, "Observer-based secure communication design using discrete-time hyperchaotic systems," *Commun. Nonlinear Sci. Numer. Simul*., vol. 19, issue 5, pp. 1424-1432, 2014.

[7] R. M. Nguimdo, R. Tchitnga, and P. Woafo, "Dynamics of coupled simplest chaotic two-component electronic circuits and its potential application to random bit generation," *Chaos*, vol. 23, 043122, 2013.

[8] J. Kengne, J. C. Chedjou, G. Kenne, and K. Kyamakya, "Dynamical properties and chaos synchronization of improved Colpitts oscillators," *Commun. Nonlinear Sci. Numer. Simulat*., vol. 17, issue 7, pp. 2914-2923, 2012.

[9] J. Kengne, J. C. Chedjou, T. Fonzin Fozin, K. Kyamakya, and G. Kenne, "On the analysis of semiconductor diode based chaotic and hyperchaotic generators: A case study," *Nonlinear Dyn*., vol. 77, issue 1-2, pp. 373-386, 2014.

[10] G. Sivaganesh, "Analytical study of an MLC circuit with quasiperiodic forcing," *Chinese Journal of Physics*, vol. 52, no. 6, pp. 1760-1769, December 2014.

[11] A. Tamasevicius, S. Bumeliene, R. Kirvaitis, G. Mykolaitis, E. Tamaseviciute, and E. Lindberg, "Autonomous Duffing-Holmes type chaotic oscillator," *Electron. Electr. Eng.- Kaunas: Technol*., vol. 5, issue 93, pp. 43-46, 2009.

[12] J. C. Sprott "A new Chaotic Jerk Circuit," *IEEE Transactions on Circuits and Systems-II Expressions Briefs*, vol. 58, issue 4, pp. 240-243, 2011.

[13] S. H. Strogatz, *Nonlinear Dynamics and Chaos: With Applications to Physics, Biology, Chemistry, and Engineering*, Perseus Books Publishing, New York, 1994.

[14] F. Kenmogne, "Generalizing of differential transform method for solving nonlinear differential equations," *Kenmogne, J Appl Computat Math*, vol. 4, issue 1, 2015.